Journal of Hydrology 527 (2015) 576–589

Contents lists available at ScienceDirect

Journal of Hydrology

journal homepage: www.elsevier.com/locate/jhydrol

Model analyses of the contribution of in-channel processes to sediment concentration hysteresis loops

Jan Pietroń [a,*], Jerker Jarsjö [a], Anna O. Romanchenko [b], Sergey R. Chalov [b]

[a] Department of Physical Geography, and the Bolin Centre for Climate Research, Stockholm University, SE-106 91 Stockholm, Sweden
[b] Faculty of Geography, Lomonosov Moscow State University, 119991 Leninskie gory, 1, Moscow, Russia

ARTICLE INFO

Article history:
Received 7 July 2014
Received in revised form 23 March 2015
Accepted 6 May 2015
Available online 14 May 2015
This manuscript was handled by Konstantine P. Georgakakos, Editor-in-Chief, with the assistance of Ehab A. Meselhe, Associate Editor

Keywords:
In-channel processes
Hysteresis
Sediment transport
In-channel storage
HEC-RAS
Tuul River

SUMMARY

Sediment concentration (*SC*)–water discharge (*Q*) relations in rivers are typically governed by multiple and relatively complex processes. Due to hysteresis effects, sediment discharges can differ for similar or equivalent water discharges, which causes scatter in empirical datasets and may decrease the predictive power of *SC* rating curves. Such hysteresis effects must therefore be understood and accounted for to make dependable predictions for river system management. The overall objectives of this study are to develop modelling approaches suitable for reproducing and predicting hysteresis effects at larger scales and to investigate the possible contribution of in-channel processes (erosion and deposition) to sediment concentration hysteresis loops. To investigate relevant field-scale conditions, we develop a one-dimensional dynamic sediment transport model of the downstream Tuul River (northern Mongolia), investigating in-channel processes along a 141 km stretch during a hydrological year. The results show that the present modelling approach can reproduce both anti-clockwise and clockwise hysteresis effects. Importantly, in-channel processes alone can cause considerable anti-clockwise hysteresis effects without being reinforced by catchment processes such as hillslope erosion. Such specific contributions from in-channel processes introduced data scatter into the sediment rating curves, decreasing their R^2-values from unity to approximately 0.5 to 0.6. More generally, possible changes in the number or magnitude of high-flow events, caused by climatic or other anthropogenic factors, could influence total sediment deposition, which was primarily found to occur during relatively short high-flow events. Such potential changes also have important implications for the possible spreading of polluted sediments.

1. Introduction

Single hydrological flow events can substantially contribute to riverine sediment transport (Smith et al., 2003; López-Tarazón et al., 2009; Ollivier et al., 2010). Knowledge on the magnitude and variability of event-based sediment loads is essential for the protection planning and management of river systems, including their contaminants and ecosystems (Lisle, 1989; Graf, 1996; Törnqvist et al., 2011; Cofalla et al., 2012; Destouni et al., 2013). In natural river systems, sediment transport hysteresis can be observed to varying extents (Lawler et al., 2006; Fan et al., 2013); thus, sediment discharge is variable for similar or equivalent water discharges. Furthermore, sediment concentration (*SC*)–water discharge (*Q*) hysteresis loops can vary from clockwise to anti-clockwise. Clockwise hysteresis loops occur when the *SC* peak arrives before the *Q* peak. The *SC* is then generally greater during the rising limb of a flow hydrograph than during the falling limb. Clockwise hysteresis loops are often related to the depletion of readily available sediment sources and the associated dilution of suspended sediment concentrations (Bača, 2008). High *SC*–*Q* skewness can occur when the bed load constitutes a considerable portion (>30%) of the total sediment load (Alexeevsky, 1998), such as in the presence of large in-channel sediment sources (e.g., submerged bars). Anti-clockwise hysteresis loops occur when the sediment delivery to the river channel is limited at the beginning of an event. These loops can, for instance, be associated with catchment processes that delay the sediment delivery from the upper portions of a river basin (Hughes et al., 2012). Furthermore, anti-clockwise loops can be a result of the delivery of fine-grained material from disturbed floodplains, including mining sites (Chalov, 2014).

The *SC*–*Q* relations in rivers are typically governed by multiple and relatively complex processes (Hudson 2003; Lawler et al., 2006; Lefrançois et al., 2007), such as hillslope erosion within catchment areas (Nadal-Romero et al., 2008; Runkui et al., 2010), sediment wave dispersion (Bull, 1997), upstream floodplain

* Corresponding author. Tel.: +46 8 16 4890.
E-mail address: jan.pietron@natgeo.su.se (J. Pietroń).

http://dx.doi.org/10.1016/j.jhydrol.2015.05.009
0022-1694/

sedimentation (Asselman and van Wijngaarden, 2002) or an abrupt erosion of river banks (Lefrançois et al., 2007). In many cases, the net effect of such varied processes is quantified empirically based on historical observation data. Commonly, these relations take the power law form: $SC = aQ^b$, where a and b are regression coefficients (Asselman, 2000). However, the above-mentioned hysteresis effects cause scatter in the empirical datasets, which must be understood and considered to enable dependable predictions for river system management. A primary challenge is therefore to identify key governing processes and their relative contribution to such hysteresis, particularly at large-catchment scales, where many of the processes are less well investigated or understood than at smaller scales (Williams, 1989; Alexeevsky, 1998; Jarsjö et al., 2012; Törnqvist et al., 2015).

For example, in addition to catchment and floodplain processes, spatiotemporal shifts in the channel characteristics, such as its cross-sectional shape, gradient and/or bed material conditions, can also potentially contribute to hysteresis in SC–Q relations (Kleinhans et al., 2007; El kadi Abderrezzak and Paquier, 2009). These in-channel changes are generally caused by natural processes, such as erosion and deposition, and reflect spatiotemporal sediment storage conditions. The exchange of sediments on a channel bed can be very dynamic under transient flow conditions (Ciszewski, 2001), particularly in relation to the longer timescales of floodplain storage (Walling et al., 1998). Although in-channel dynamics clearly contribute to the variability in sediment yield along rivers (Smith and Dragovich, 2008) through erosional/depositional processes that cause differences between upstream and downstream sediment loads (Owens et al., 1999; Smith et al., 2003), questions remain regarding whether and to what extent in-channel processes contribute to hysteresis effects.

The overall objectives of this study are to develop modelling approaches suitable for reproducing and predicting hysteresis effects at larger scales and to investigate the possible contribution of in-channel processes to sediment concentration hysteresis loops. These aims also include more detailed assessments of the dynamics of in-channel sediment bed storage and gradation changes throughout a hydrological season and within single hydrological events. To this end, we use a one-dimensional dynamic sediment transport model supported by field observations in the Tuul River (northern Mongolia), which is characterised by a natural hydrological regime unaffected by engineered structures.

2. Materials and methods

2.1. Site description

The Tuul River is located in the Mongolian (upper) portion of the Selenga River Basin, which collects the majority of the runoff within the Lake Baikal Basin (Fig. 1a), located in southern Siberia (Russian Federation). The Tuul River flows from the Khetei mountain range to the Orkhon River, passing through the most populated area in Mongolia, the city of Ulan Bator, in its upstream portion. The area of the Tuul River Basin is approximately 50,000 km^2. The annual average air temperature at the Ulan Bator station is −0.8 °C, and the monthly means vary between −21.5 °C in January and 17.1 °C in July. The annual precipitation of the basin varies between 275 mm in its middle reaches and over 400 mm in the most upstream and downstream reaches of the river. The precipitation in the basin occurs mainly as rainfall in the warm May–August period. The annual mean discharge of the Tuul River at the Ulan Bator gauging station is 27 m^3/s, and the maximum recorded discharge since 1945 is 1580 m^3/s (Davaa and Odgarav, 2012).

During winter (November–March), the Tuul River channel is covered with thick ice, and its discharge is negligible. However, recent observations indicate a decreasing duration and thickness of the ice cover (Punsalmaa et al., 2004), which may reflect climatic changes in the region. Other indicators of climate change in the region include extended low-water periods in the lower (Russian) part of the Selenga River in recent decades (1976–1982 and 1996–2011; Chalov et al., 2015; Berezhnykh et al., 2012; Shimarayev and Starygina, 2010). Such hydrological changes have also been observed in the upper (Mongolian) portion of the Selenga River (Garmaev and Khristovorov, 2010; Davaa and Odgarav, 2012). Long-term hydrological data (1945–2012) for the Tuul River and the downstream sections of the river network (Orkhon River) demonstrate a low-water period since 1996 (Fig. 2a). However, in the Tuul River Basin, higher discharge conditions were observed during the most recent hydrological years (2012 and 2013; Centre of Register of Hydrotechnical Constructions, 2014). In addition, the annual maximum discharges have decreased since the mid 1990s (Fig. 2b). This is consistent with the observed pattern in the Selenga River Basin, where the maximum discharges have decreased and the minimum discharges have increased, which may reflect permafrost thaw in the basin (Törnqvist et al., 2014).

This study focuses on a 14 km long reach (called the focus reach) located approximately 104 km from the confluence of the Tuul and Orkhon rivers (Fig. 1c). The modelled reach of the river was much longer (Fig. 1b) than that to sufficiently separate the focus reach from the model boundaries and their influences (see also Section 2.2.4). The entire modelled reach of the Tuul River extends 245 km upstream of the confluence with the Orkhon River (Fig. 1b).

The geomorphology of the valley of the downstream Tuul River varies from quite wide with relatively flat floodplains (especially in the upper part) to narrow and more v-shaped in hilly areas. The average slope of the focus reach is 0.0004 (m/m), which is preceded by a long reach with an average slope of approximately 0.001 (see the Supplementary Information for a more detailed description). The channel of the focus reach is meandering, which is also the case for approximately 68% of the modelled reach of the Tuul River. This channel pattern is associated with abundant horizontal and vertical channel changes (Alexeevsky et al., 2013). In its most downstream reaches, the Tuul River crosses a mountainous area. This portion of the river has an incised channel containing extended straight reaches, which indicate stable channel conditions. The topography and vegetation of the Tuul River Basin is typical for a grassland steppe, with occasional shrub cover in the vicinity of water bodies. The natural steppe ecosystem and landscape of the downstream Tuul River valley, however, is disturbed by expanding placer gold mining. As shown in Fig. 1b, the mines are distributed over a large distance beginning just upstream of the focus reach. Previous studies of the mining activity indicate severe environmental impacts on the bodies of water downstream of the Tuul River and on Lake Baikal (Ferrington, 2000; Stubblefield et al., 2005; Byambaa and Todo, 2011; Thorslund et al., 2012).

2.2. Numerical modelling

HEC-RAS 4.1 is a one-dimensional modelling software package that allows the performance of four different river analyses: (1) steady flow, (2) unsteady flow, (3) water quality (organic matter) and (4) movable boundary sediment transport computation, which is used in this study. All four components of the model use common geometric data and common geometric and hydraulic computation routines (USACE, 2010a). The HEC-RAS sediment transport module has been successfully implemented in studying both relatively short (Zhang and Duan, 2011) and long, exceeding 300 km,

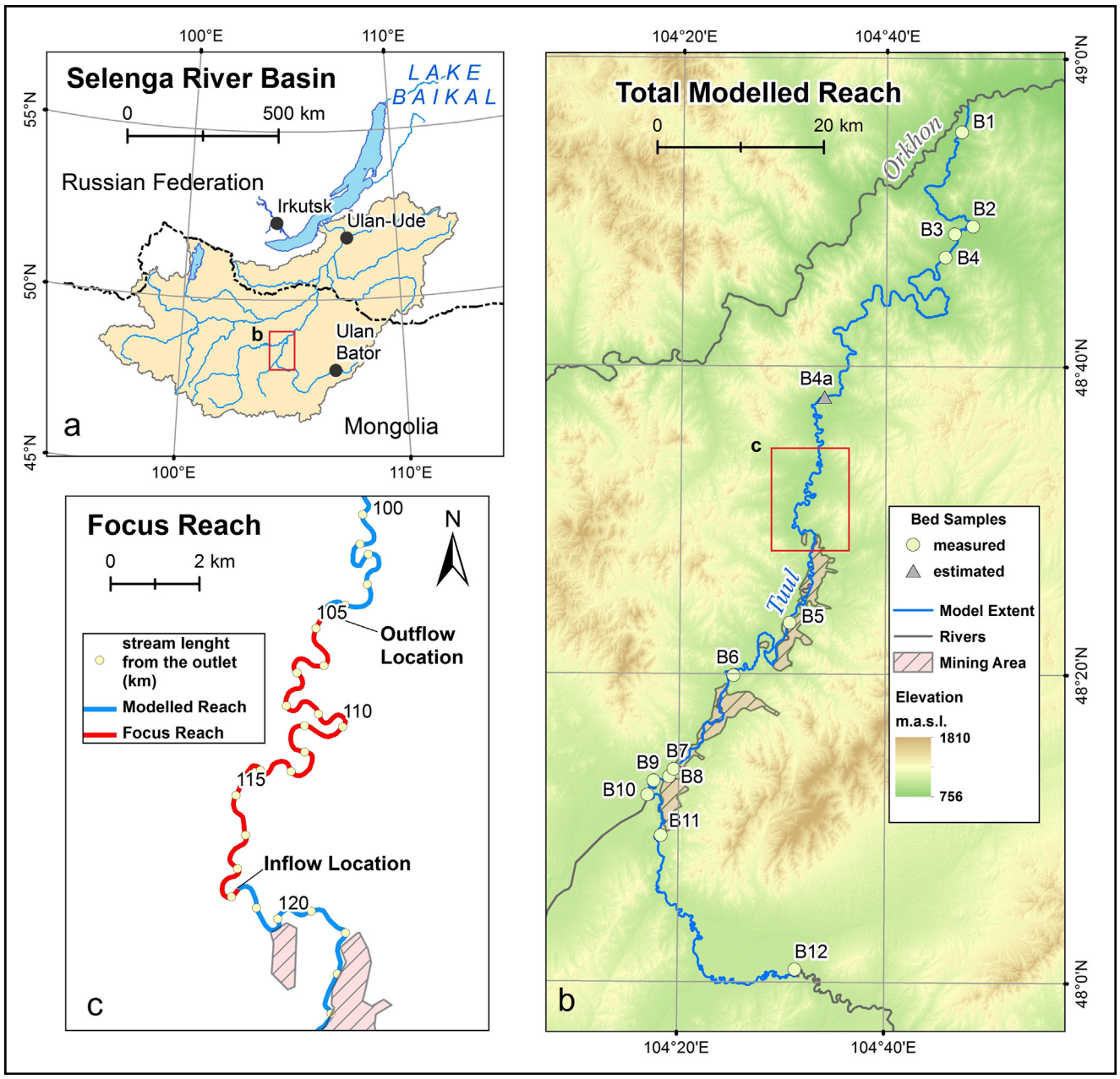

Fig. 1. (a) The Selenga River Basin, indicating the location of the modelled reach extent; (b) the downstream Tuul River and modelled reach extents with the location of the focus reach; (c) the focus reach extent.

river reaches (Pereira et al., 2009; Adams and Chen, 2010). The capabilities of this sediment transport model are often commended due to their user-friendly interface and wide range of available outputs (Gibson et al., 2006; Herman et al., 2007). To estimate sediment transport for transient flow conditions, HEC-RAS uses a quasi-unsteady approach, which assumes that an event or a period of records is calculated as a series of steady flows. This assumption has been shown to produce similar results to those of models based on unsteady flow algorithms (Hummel et al., 2012). The primary input data for the sediment transport computations conducted here are (1) bed material, (2) stream geometry, (3) upstream and downstream flow boundary conditions (BC), and (4) upstream sediment load boundary conditions. The development of the downstream Tuul River model was divided into three steps: (1) river geometry development, (2) flow model development and (3) sediment transport model development (Fig. 3).

2.2.1. Data acquisition and processing

Most of the measurement data used in the model were obtained from two field campaigns in the Zaamar region: (1) 24th July to 4th August 2011 and (2) 18th June to 31st June 2012. Topographical data were obtained from a 90 m resolution DEM (Digital Elevation Model) from USGS (SRTM 90m; USGS, 2012a). The river bathymetry was acquired by measuring the depth at cross-sections at locations B1, B6 and B12 (Fig. 1b) in the Tuul River study reach. The measurements were conducted during the field campaign in 2011. The centreline of the river was derived from LANDSAT images representing the area of the study site for 11th July 2011 (USGS, 2012b).

In this study, we reproduce sediment transport conditions typical for the Tuul River using discharge data from a recent hydrological year (2011) from the Ulan Bator gauging station, which were provided by the Mongolian Institute of Meteorology, Hydrology

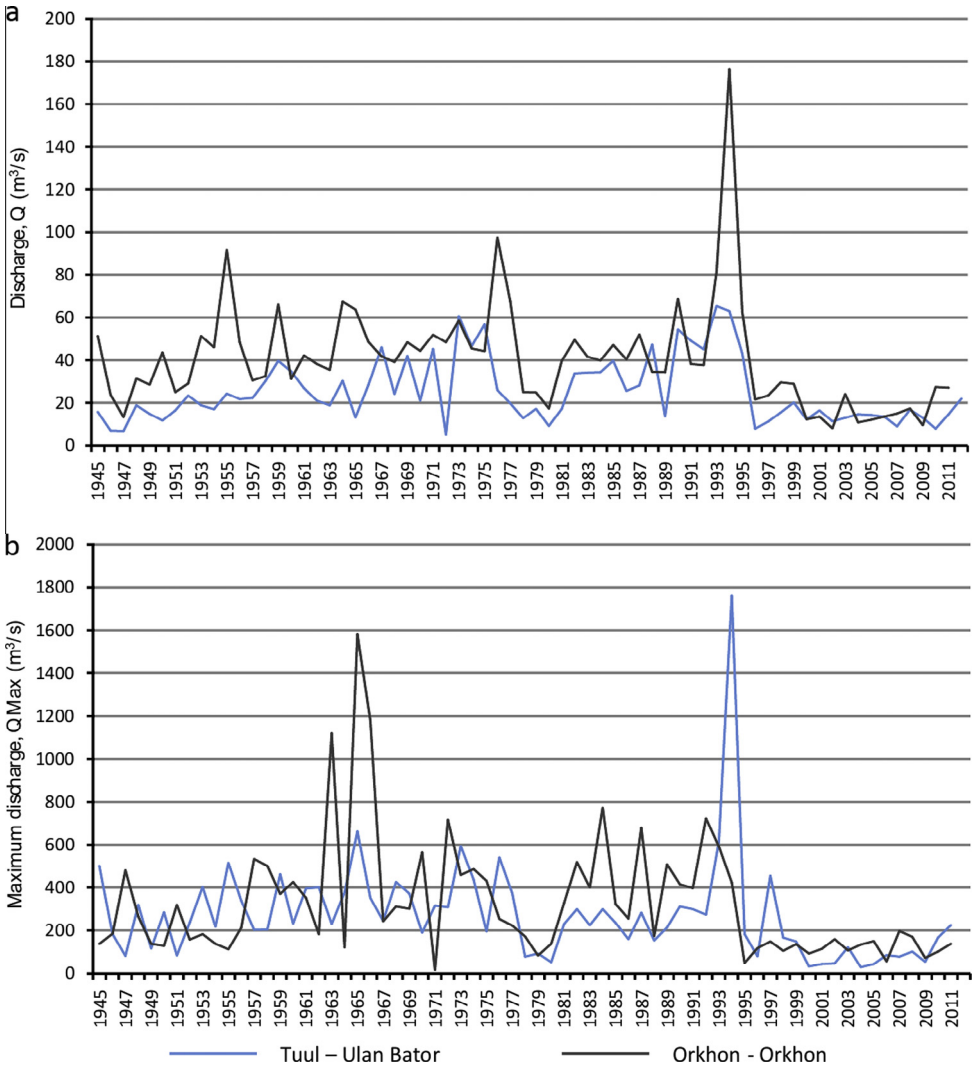

Fig. 2. Long-term changes in the (a) annual and (b) maximum discharges, *Q*, in the Tuul and Orkhon rivers (Garmaev and Khristovorov, 2010; Davaa and Odgarav, 2012).

and Environment (Davaa, 2012). The data represent hydrological conditions of the most recent decades (Fig. 2) and were used to prescribe the flows at the upstream boundary of the model. Previous measurements have shown that the Tuul River flow is essentially unchanged between the gauging station and the region where the upstream boundary of the model is located (Battulga et al., 2009).

The velocity–discharge profiles used in the flow model calibration were measured at locations B6 and B12 during the field campaign in June 2011 and at B1, B5–7 and B11–12 during the field campaign in June 2012. The measurements were taken at a minimum of three subdivisions in a river profile using a propeller-type current meter. Mean monthly water temperature data, required for the sediment transport model, were taken from Altansukh (2008).

The bed sediment was investigated at 12 locations (Fig. 1b), of which 11 were collected from the Tuul River reach during the 2012 field campaign. The samples were collected using either (1) a so-called "Russian corer" (for catch-and-close samples of the material) or (2) a cylindrical steel vessel (for coarse bed material). In the first method, the maximum depth of the samples was 10 cm. The second method was based on removing approximately 5 cm of the bed material by dragging the vessel in the direction of the river current. Accounting for missing bed sampling in relatively inaccessible regions, we assumed that in the uninvestigated region (location B4a in Fig. 1b), the bed material gradation is proportional to the channel slope conditions. Hence, location B4a is represented by material similar to that found at locations B1–B3 and B6. All of these locations are characterised by a relatively steep slope of the channel, exceeding 0.001.

The measured bed samples from all of the locations were divided into ten sediment grain size classes using sieving analysis. The internal boundaries of the sediment grain size classes followed the size limits of the sieves. Due to limiting information from the field, it was assumed that the lower limit of the finest sediment grain size class was 0.062 mm (the lower limit of very fine sand in HEC-RAS). Later, the analysed bed material information was applied in the model. This process required some of the default HEC-RAS sediment classes to be adjusted to the size boundaries of the sediment classes measured using the sieving analysis. Hence, the "settling depth" factor, which controls the vertical distribution of each class in the water column (Gibson et al., 2010), was also adjusted for each new class. The specific gravity of the bed material was also changed from the HEC-RAS default of 2.65 to 1.91, which was measured in the upstream portion of the studied reach. In the final step, the information regarding the bed material at the sampling locations was interpolated along the modelled reach using the default HEC-RAS interpolation method.

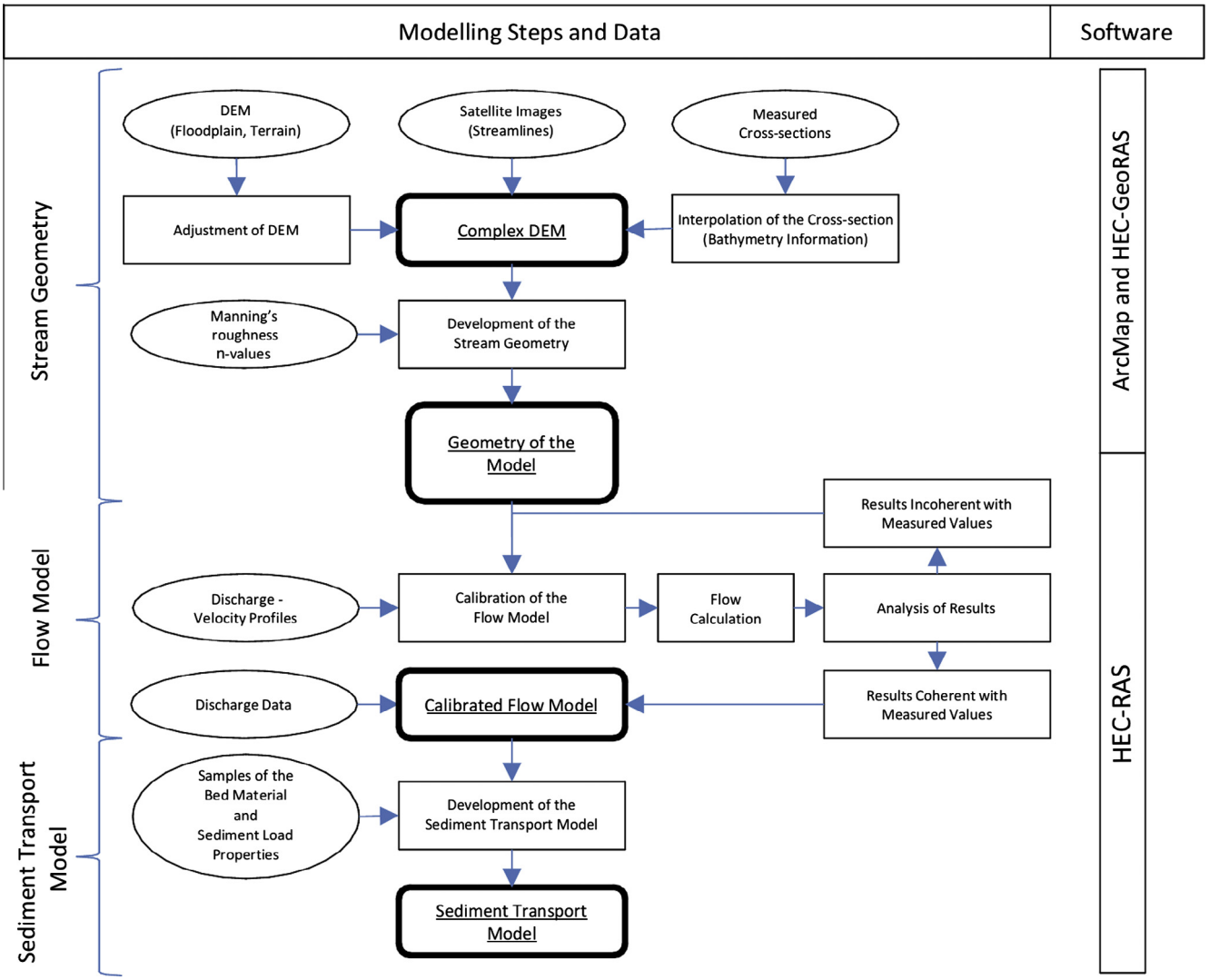

Fig. 3. Chart illustrating the steps of the development of the downstream Tuul River model.

Hence, the above procedure is measurement based, using an information snapshot from the sampling campaign. However, the natural characteristics of the bed material can vary with time. Therefore, a given hydrograph can result in different erosional/depositional patterns depending on the initial state of the bed, such as the abundance or deficiency of the most conveyed material. We therefore investigate two hypothetical cases with sediment gradations that are different from the measurement-based case. The two additional scenarios imply a relative abundance (scenario A) and deficiency (scenario B) of the finest analysed material in the bed of the focus reach. However, in the two scenarios, all of the sediment classes need to be defined, not only the finest analysed class. To obtain a gradation that reflects typical conditions for the Tuul River, we base the full gradation of the additional scenarios on the observed (sampled) conditions in the downstream Tuul River. The observations considered have high (scenario A) and low (scenario B) proportions of the finest analysed fraction. The general characteristics and results of the additional modelling scenarios (A and B) are presented in the Supplementary Information (Table S-1).

2.2.2. River geometry development

The geometry of the downstream Tuul River was developed using HEC-GeoRAS 4.3, an extension to the GIS program ArcMap 9.3. The floodplain area and the slope of the stream were derived from the DEM. The bathymetry mesh of the river was created using the measured cross-sections and the delineated centreline of the river. The width of the channel was assumed to be constant at 52 m, which is consistent with the average width of the measured cross-sections.

Cowan's method was used to estimate Manning's roughness coefficients (n) along the Tuul River channel and floodplains. The n-values reflect local energy losses and were estimated from $n = (n_b + n_1 + n_2 + n_3 + n_4)m$, where n_b is a base value of the coefficient for a straight and smooth channel in natural materials; m is a meandering correction factor; and n_1, n_2, n_3, and n_4 are correction factors for (1) surface irregularity, (2) shape and size variability of a channel, (3) obstructions, and (4) vegetation and flow conditions, respectively (Arcement and Schneider, 1984).

The geometry of the downstream Tuul River that was imported from HEC-GeoRAS to HEC-RAS was composed of approximately 1300 cross-sections along the 245 km of the modelling reach (62 cross-sections within the focus reach of the study). The spacing between the cross-sections was set to be denser in the more meandering locations of the river (see the Supplementary Information for a more detailed description of the model geometry creation).

2.2.3. Flow model development and calibration

Daily discharge data for the year 2011 were applied as the upper BC to the model. There was no discharge recorded between

January and early March 2011, most likely due to a thick ice cover. There are a few minor tributaries and one larger tributary, the Haruuhn River, along the modelled reach. We assume that the relation between the monitored and unmonitored flow is the same as the relation between the monitored and unmonitored catchment areas (see Destouni et al., 2008; Jarsjö et al., 2008). Therefore, the unmonitored discharge increases in proportion to the catchment area increment according to the following:

$$Q^{um} = Q^{m}\frac{A^{m} + A^{um}}{A^{m}} \quad (1)$$

in which Q^m is the monitored discharge, Q^{um} is the unmonitored discharge at a point downstream of the monitored one, A^m is the catchment area of the monitored discharge, and A^{um} is the catchment area of the unmonitored discharge. The calculated discharge increments were applied in the model assuming that the discharge increase is divided equally among all modelling cross-sections of each considered sub-catchment (see the Supplementary Information for a more detailed description).

The flow model was calibrated using sets of velocity-discharge profiles acquired in 2011 and 2012. The calibration procedure involved adjusting Manning's n-values to obtain similar measured average stream velocities during correspondingly applied discharge conditions.

2.2.4. Sediment transport model development

Different sediment transport quantification methods, such as Ackers-White, Engelund-Hansen, Toffaleti, and Yang and Wilcock, have been developed under different limiting assumptions (Camenen and Larroudé, 2003; Benjankar and Yager, 2012) and may therefore yield different results for a particular river reach to the extent that some results may be inconsistent with observed data (Młynarczyk, 1996; Yang, 2002). In the present Tuul River application, the Toffaleti (USACE, 2010b) function for sediment transport was found to be the most appropriate because it has been developed for medium and large rivers that fit the characteristics of the Tuul River. The Toffaleti formula is a function of the geometric characteristics of the channel, average velocity, sediment grain size, an empirical exponent (describing the relationship between the sediment and hydraulic characteristics) and water temperature.

The bed sorting method, which computes changes in bed material gradation with time and limits erosion of the bed, was set to Exner 5 (USACE, 2010b). This method creates two layers out of the active layer of the input bed material, which simulates the effect of bed armouring protecting deeper material from erosion (Gibson et al., 2006). Fall velocity, which controls the depositional speed of particles, was established by another method developed by Toffaleti (USACE, 2010b).

The varying capacities for material transport are calculated for each sediment grain size class separately. These capacities are calculated based on the transport potential of the grain size (calculated with the transport equation) multiplied by the fraction of each sediment grain size class in the active layer of the channel bed (USACE, 1993). Hence, when the sediment deliveries are greater than the transport capacity of the given material, deposition of this material occurs. Conversely, if the transport capacity is greater than the deliveries, erosion occurs. Thus, according to the model assumptions, the erosion/deposition rates depend on both the incoming sediment loads and the in-channel sediment storage.

Because the model was developed to simulate the in-channel sediment transport and erosional/depositional dynamics, the only supply of sediment in the model was from the bed material of the river. The incoming sediment load was obtained by setting the upper BC to "equilibrium load" (see USACE, 2010a). The stretch between the upper BC of the model and the focus reach acted as an adaptation reach of the model (127 km long). In other words, the sediment load flowing into the focus reach was primarily a result of the upstream erosion of in-channel bed sediment supplies rather than the upper sediment load BC applied in the model. The robustness of the focus reach results with regard to assumed conditions at the upper boundary was evaluated through prescribing extremely low (0 t/day) and high (700 t/day) inflowing sediment loads at this boundary, considering also the full range of studied discharges. It was shown that the average difference between sediment concentrations at the focus reach due to the different prescribed boundary loads was small (median value of 4.5%), despite the large difference at the boundary. Furthermore, a previous comparison between measured and modelled sediment concentrations based on the same model and application site as considered here (Chalov et al., 2015), showed that the model can reasonably reproduce absolute values of concentration; the median ratio between measured and modelled concentrations was found to be less than 2, whereas the ratio between maximum and minimum concentrations that occurred under the investigated condition was relatively high (50).

2.3. Hydrological analysis

To separate the flow events from the base flow periods of the stream hydrograph, the local-minimum method was used. This method determines the base flow by linking the minima flow between the events (Sloto and Couse, 1996). To distinguish the major flow events from the others, we define the primary events as those with at least double the current base flow.

In the analysis of the model results, we define net erosion/deposition (net storage) as the difference in the sediment mass stored within the channel of the focus reach between the beginning of the studied hydrological period and the considered point of time. Furthermore, daily net erosion/deposition refers to the sediment mass difference within a single day of the hydrological period. The total daily erosion during a period of time was calculated as the sum of erosion (with a value of zero for days showing no erosion or deposition) in the considered period.

3. Results

3.1. Discharge, erosion and deposition

Discharge (Q) representing the inflow to the focus reach and the results of the modelled net erosion/deposition (net storage) are presented in Fig. 4 for all sediment grain size classes. The hydrograph separation distinguished 16 peak flow events during the hydrological period (dark blue colour in Fig. 4). Five of these events were classified as major flow events (E1–E5). The major flow events E1–E3 and E4–E5 occur in sequence. There is a 13-day lapse between events E3 and E4. Two minor events occur during that time. The average Q of the hydrological period (April-December 2011) was 28 m^3/s. The maximum Q was 170 m^3/s, occurring during the last event, E5. The event E1 had the lowest peak of the major flow events, with Q equal to 71 m^3/s. The other, eleven minor events are characterised with peak Q varying between 12 and 65 m^3/s.

The model results indicate that the particles in most of the sediment grain size classes are subject to a net deposition of sediment particles over the hydrological period (Fig. 4). The highest deposition in the 14 km stretch considered is estimated for the sediment grain size class no. 2 (0.25–0.50 mm) (red dashed curve in Fig. 4), with a net deposition of approximately 7.4 kt over the hydrological period. The final change in sediment net storage for all size classes

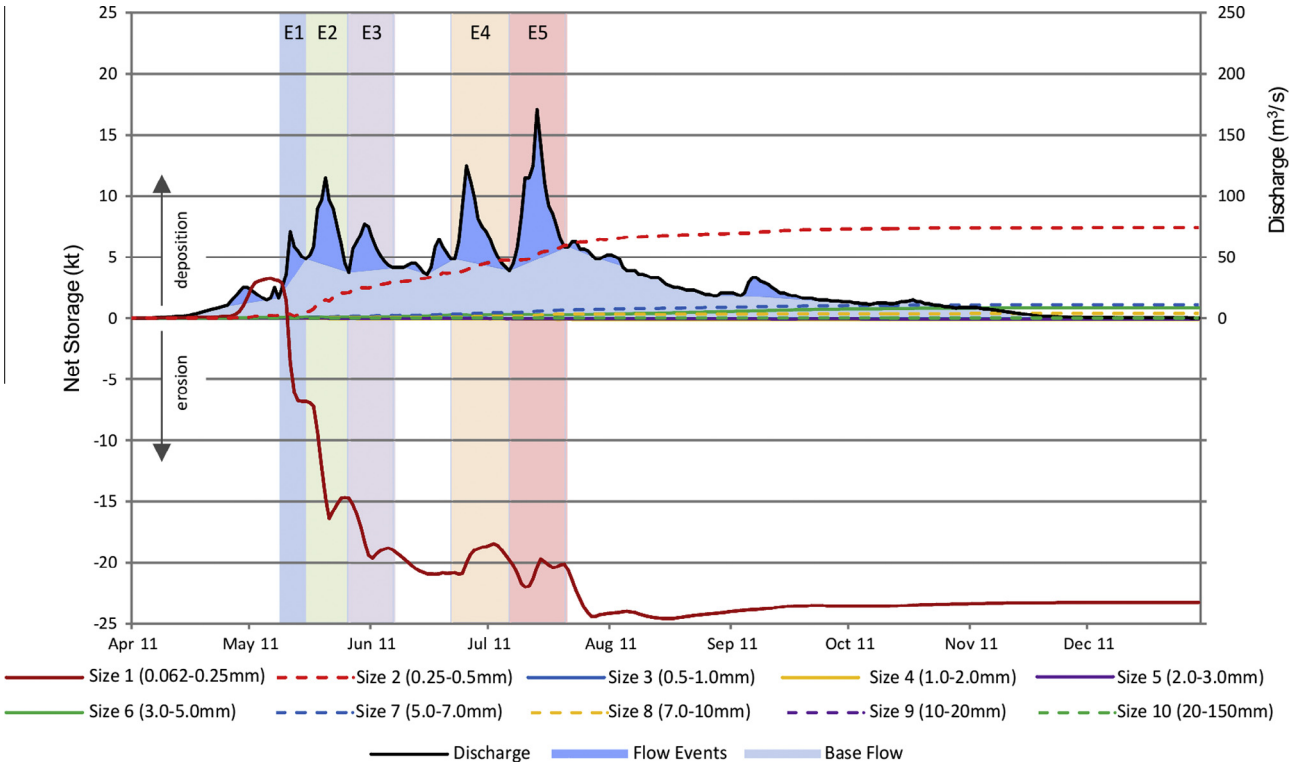

Fig. 4. Hydrograph for the focus reach with the flow events separated from base flow and net storage in the focus reach for all sediment grain size classes. The major flow events, E1–E5, are highlighted with colours. (For interpretation of the references to colour in this figure legend, the reader is referred to the web version of this article.)

however, is −14 kt, which corresponds to approximately 9.0% of the total annual sediment inflow to the focus reach. The negative number is due to a considerable net erosion of 23 kt of fine sediment from grain size class no. 1 (0.062–0.25 mm) (red solid curve, Fig. 4). This material, which initially represents 16% (see Fig. 5 for the full gradation curve of the initial bed material at the focus reach) of the bed volume, shows dynamic erosional/depositional patterns throughout the hydrological period. For instance, from April to early May, 3.3 kt of this sediment grain size class was estimated to be deposited in the reach. Subsequently, considerable erosion occurs, beginning during event E1 and continuing through event E3. Then, for the next major events, E4 and E5, the magnitude of erosion decreases and deposition increases. After the period of the major flow events, the curve of the sediment grain size class no. 1 gently increases, indicating a low rate of net deposition on the bed. In general, the finest sediment grain size class dominates the overall dynamics of sediment transport and the total sediment erosion and deposition in the focus reach and the entire modelled reach, which is consistent with available measurement data. More specifically, according to the model results for locations where measurement data was available (B11, B7 and upstream part of the focus reach; Fig. 1b and c), the finest analysed sediment fraction accounted for 92–99% of the sand fraction (0.062–0.1 mm) at discharges between 11 and 55 m^3/s. The measurements of the suspended sediment load, conducted in June 2012 and September 2013, confirm that the fine sediment fraction (0.05–0.25 mm; e.g. similar to the finest modelled fraction), account for a very large part (96–100%) of the sand fraction in suspension (0.05–1.0 mm) for the same range of discharges.

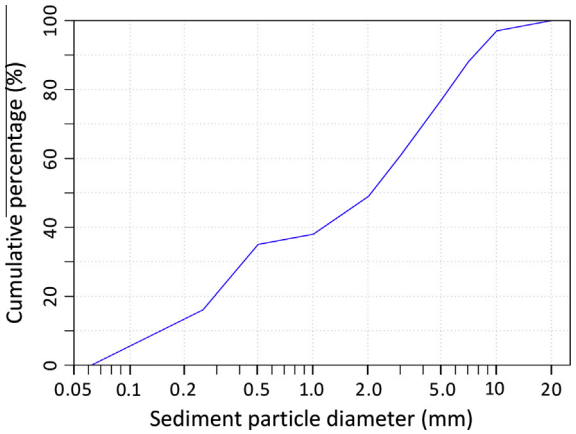

Fig. 5. Gradation curve of initial bed material at the focus reach.

Out of the 279 days considered (April–December 2011), net deposition is estimated to occur on 206 days (74%) and net erosion on 73 days (26%). The model furthermore indicates that the major flow events are responsible for 83% of the total daily net erosion, although this erosion occurs only during 12% of the hydrological period (Fig. 6a and b). The greatest daily net erosion (71%) occurs during the first major events, E1–E3, among which flow event E1 has the highest erosion rate (30% of the total erosion in 1.8% of the time). The contribution of the last major flow events, E4–E5, to the total daily net erosion is not considerable (12% of the total erosion in 4.3% of the time). Approximately 14% of the total daily net erosion occurs during the 11 minor events, which in total constitute 5.4% of the hydrological period. During the base flow in spring and autumn, very little erosion occurs (3.0% of the total erosion in 9.0% of the time).

The major flow events are estimated to be responsible for 56% of the total daily net deposition, which occurs during 9.0% of the hydrological period (Fig. 6c and d). The greatest daily net deposition occurs during the two last major events E4 and E5 (36% of the total deposition in 5.0% of the time). The major flow events

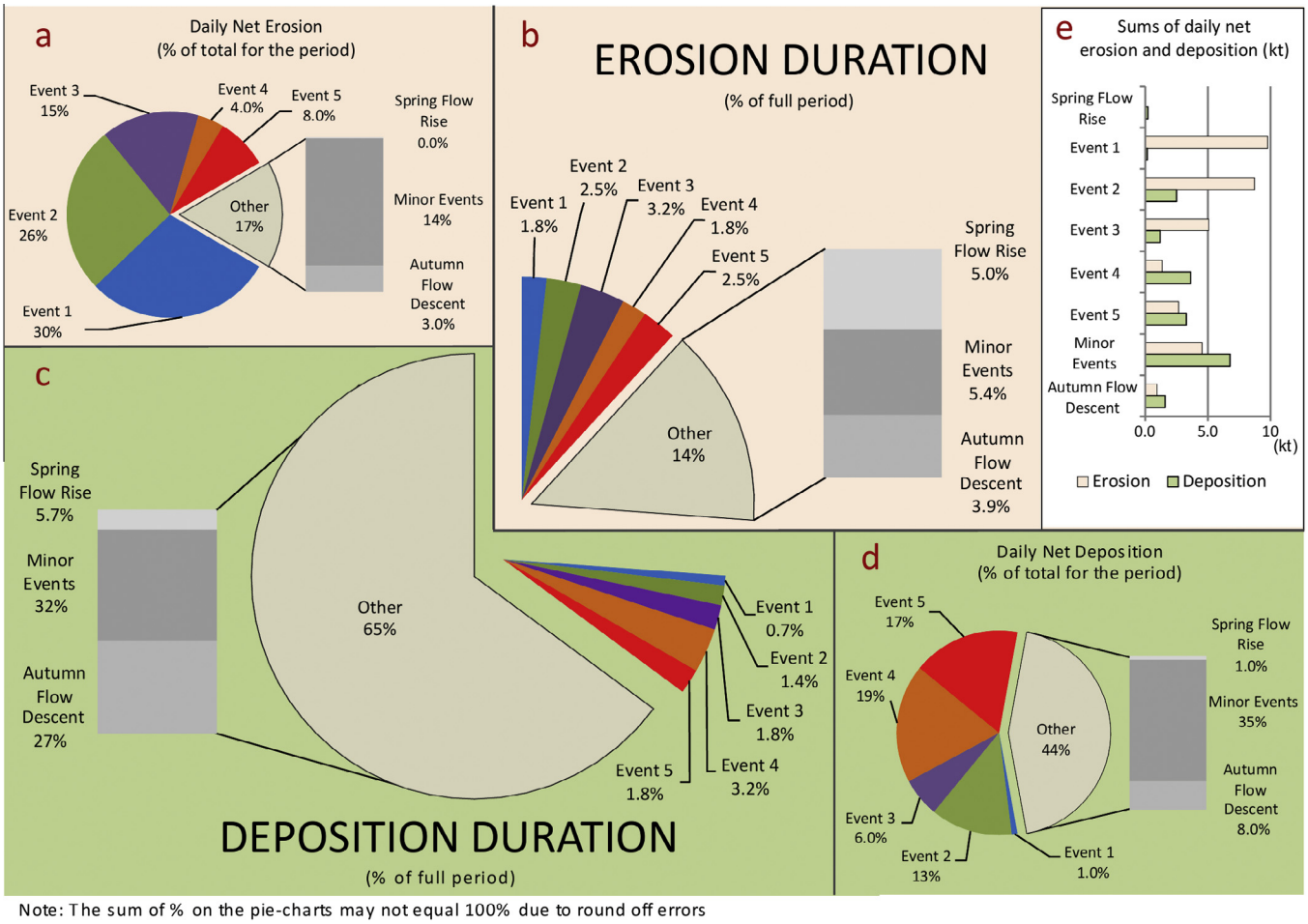

Note: The sum of % on the pie-charts may not equal 100% due to round off errors

Fig. 6. High flow events at the focus reach as: (a) percentage of the total magnitude of daily erosion, (b) percentage of time of estimated daily net erosion, (c) percentage of time of estimated daily net deposition, (d) percentage of the total magnitude of daily net deposition; (e) the magnitude of the daily net erosion and deposition in kt.

E1–E3 contribute less to the total daily net deposition (20% of the total deposition in 3.9% of the time). The 11 minor events contribute more to the total daily net deposition than to the total daily net erosion (Fig. 6e) and are responsible for 35% of the total daily net deposition, which constitutes 32% of the hydrological period. The base flow in spring and autumn contributes only with a small part of the total daily net deposition (9.0% of the total deposition in 33% of the time).

3.2. Cumulative total sediment load

In the cumulative total sediment load (*CTSL*) curves in Fig. 7, there is a negative difference in *CTSL* between the outflow location (OL) and the inflow location (IL) of the focus reach before the first major flow event E1. This difference is caused by the net deposition of the finest studied sediments (grain size class no. 1) in the focus reach, which can also be seen in Fig. 4 (red solid curve). Due to erosion in the focus reach during the major flow event E1, the increase in *CTSL* is nearly two times greater at the OL than at the IL (Fig. 7). Therefore, the difference in *CTSL* between the OL and the IL ($\Delta CTSL$) increases. The major flow events E2 and E3 also result in increases of $\Delta CTSL$. Due to prevailing erosion during the first three major flow events, the $\Delta CTSL$ changes from −3.5 kt to 16 kt. Between events E3 and E4, there is a slight increase in the $\Delta CTSL$ (Fig. 7), which indicates minor erosion during that time. Prevailing deposition in the focus reach during the major flow events E4 and E5 decreased downstream sediment transport. Therefore, the $\Delta CTSL$ changes from 17 kt to 14 kt (a change of approximately 3.0 kt). Until the end of the hydrological period, the $\Delta CTSL$ increases and decreases due to alternating erosion and deposition. Hence, the final $\Delta CTSL$ for the hydrological period equals 14 kt, which corresponds to 8.0% of the *CTSL* at the OL. In addition, cumulative sediment load of each grain size class at IL and OL is presented in the Supplementary Information.

3.3. Sediment concentration hysteresis loops

The water that flows into the focus reach at the IL is characterised by the common anti-clockwise hysteresis loops of sediment concentration (*SC*; blue curves, Fig. 8a) during all major flow events. Hence, in all cases, the *SC* peaks at the IL lag behind the discharge peaks. For instance, for the major flow event E1 (May 09–15, 2011), the *SC* peak occurs on the final day of the event and is delayed in relation to the *Q* peak that occurs on day 3 of the event. In contrast, at the OL, the *SC* hysteresis loop for the major flow event E1 changes to clockwise (red curve, Fig. 8a). The *SC* peak at the OL occurs on the same day as the discharge peak. The differences in *SC* between the two locations (IL and OL) are related to the vast erosion of the channel bed in the focus reach (Fig. 8b). For event E1, the daily net erosion of the bed sediment precedes a very low net deposition that occurs during the final two days of the event. The daily net erosion peak (5.1 kt) occurs on the same day as the *Q* peak and the *SC* peak at the OL. The second major flow event, E2 (May 16–26, 2011), is also characterised by a delayed *SC*

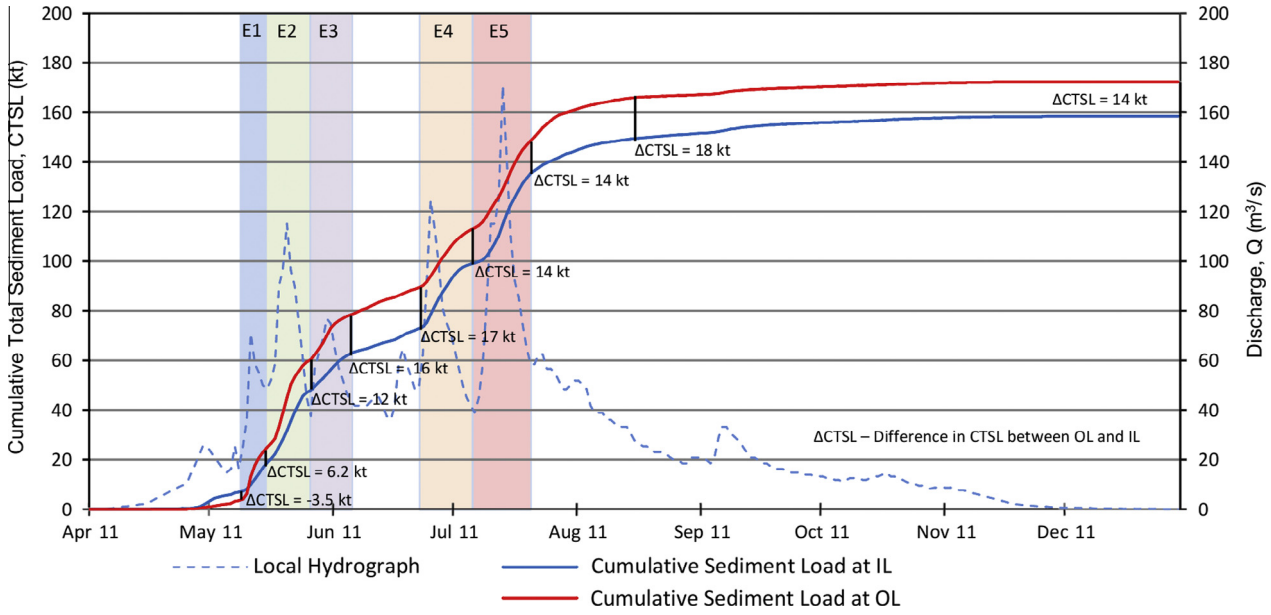

Fig. 7. *CTSL* for the IL (blue curve) and the OL (red curve), with the difference between the OL and the IL (*ΔCTSL*) indicated with black lines; the dashed blue line indicates discharge in the focus reach. The major flow events, E1–E5, are highlighted with colours. (For interpretation of the references to colour in this figure legend, the reader is referred to the web version of this article.)

peak in relation to the *Q* peak at the IL (Fig. 8a). Event E2 is characterised by clockwise *SC* hysteresis loop at the OL. Bed erosion occurs during the early stage of the flow event (Fig. 8b). At the OL, the *SC* peak and the highest daily net erosion (2.6 kt) occur a day before the *Q* peak. The final five days of the event are characterised by a daily net deposition of sediment (max. 0.9 kt). The third major flow event, E3 (May 27–June 09, 2011), shows patterns of *SC* hysteresis loops and daily net erosion/deposition similar to those of event E2 (Fig. 8). Prevailing erosion during the major flow events E1–E3 resulted in changes in the gradation of the active layer bed material. In particular, the fraction of grain class no. 1 decreased from 12% to 2.0%, indicating depletion of this most commonly transported material.

The major flow events E4 (June 23–July 06, 2011) and E5 (July 07–18, 2011) are characterised by anti-clockwise *SC* hysteresis loops at both the IL and the OL (Fig. 8a). At the IL, the major flow event E4 begins with rapidly increasing *Q* and *SC*. During most of the event, the *SC* values at the OL are lower than at the IL. The difference in *SC* between the two studied locations (IL and OL) is associated with the daily net deposition of sediment in the focus reach, which begins early in the event and generally continues throughout (Fig. 8b). When the deposition begins, 2.0% of the sediment in the active layer is from grain size class no. 1. After eight days of net daily deposition, the fraction of the sediment in the active layer from grain size class no. 1 increases to 3.8%. Daily net erosion occurs during the final four days of the major flow event E4. More generally, the *SC* values in the early stage of events E4 and E5 are clearly lower than those in the final stages. Moreover, the *SC* peak for event E5 occurs on the final day of the event. However, in contrast to event E1, the *SC* hysteresis loop at the OL remains anti-clockwise during event E5. Additionally, there is a significant difference in the pattern of the anti-clockwise *SC* loops between the OL and the IL. The first days of event E5 are characterised by higher *SC* values at the OL than at the IL, which is a result of daily net erosion (max. 0.80 kt) occurring during that time (Fig. 8b). Subsequently, during the few days of high *Q*, the *SC* loop at the OL has a lower *SC* than at the IL (Fig. 8a), which is a result of daily net deposition (max. 1.3 kt). On the final day of event E5, 3.9% of the sediment in the active layer is from grain class no. 1. One can furthermore note that deposition occurred on the day of *Q* peak in events E4 and E5, whereas erosion occurred in event E2. This can be explained by a limited bed sediment availability of the grain size class no. 1 prior to the high flows of events E4 and E5.

4. Discussion

For the hydrological period considered, which covers the total discharge of the Tuul River in 2011, the change in in-channel storage over the focus reach (also expressed as *ΔCTSL* in Section 3.2) corresponds to 8.0% of the cumulative sediment load at the OL. This relationship can be compared with that observed for other rivers that have relatively undisturbed hydrological flow regimes. The in-channel storage at the Isábena River (Spain) corresponds to 5.0% of the annual sediment load (López-Tarazón et al., 2012). Furthermore, the annual change of the in-channel storage corresponds to 9.0% and 10% of sediment delivery in the rivers Ouse and Wharfe (UK), respectively (Walling et al., 1998). Hence, the modelled magnitude of the in-channel storage in the Tuul River is similar to the observed storage in other unregulated rivers.

The storage change discussed above suggests a net erosion of the Tuul River sediments. These results were obtained assuming that the bed material was approximately 16% relatively fine material, which is consistent with the on-site observations from summer and autumn. However, a hydrological year can in theory begin with different fractions of fine material in the bed, depending on the previous hydrological conditions. Therefore, the possible effects of such differences are discussed below. Notably, additional scenarios with more (40%; scenario A) and less (1%; scenario B) fine bed material than the 16% in the base scenario show that the same hydrograph can yield both negative and positive net storage changes (sediment budgets) at the end of the hydrological period. Although an abundance of the fine material (scenario A) increases the rate and magnitude of erosion, as expected, a deficiency (scenario B) increases the overall role of deposition. Consequently, scenario A yielded negative morphological changes (−7.1 kt/year/km), whereas scenario B yielded positive ones (4.9 kt/year/km). In both cases, the changes were relatively high in comparison with the

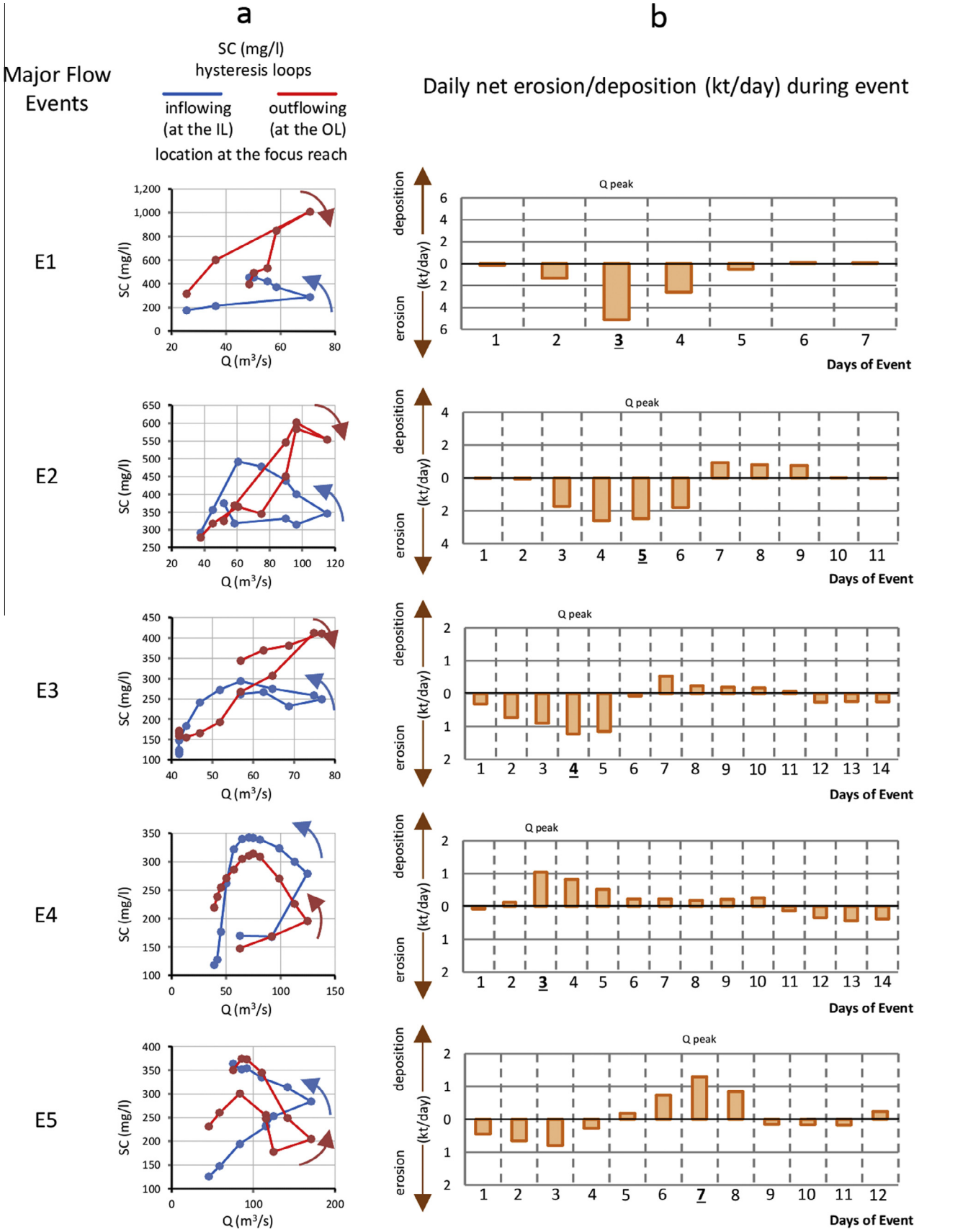

Fig. 8. (a) *SC* hysteresis loops for the major flow events at the IL (blue curve) and the OL (red curve); (b) daily net erosion/deposition (kt/day) in the focus reach for each day of the major flow events; bolded and underlined numbers of days indicate the peak discharges of the events. (For interpretation of the references to colour in this figure legend, the reader is referred to the web version of this article.)

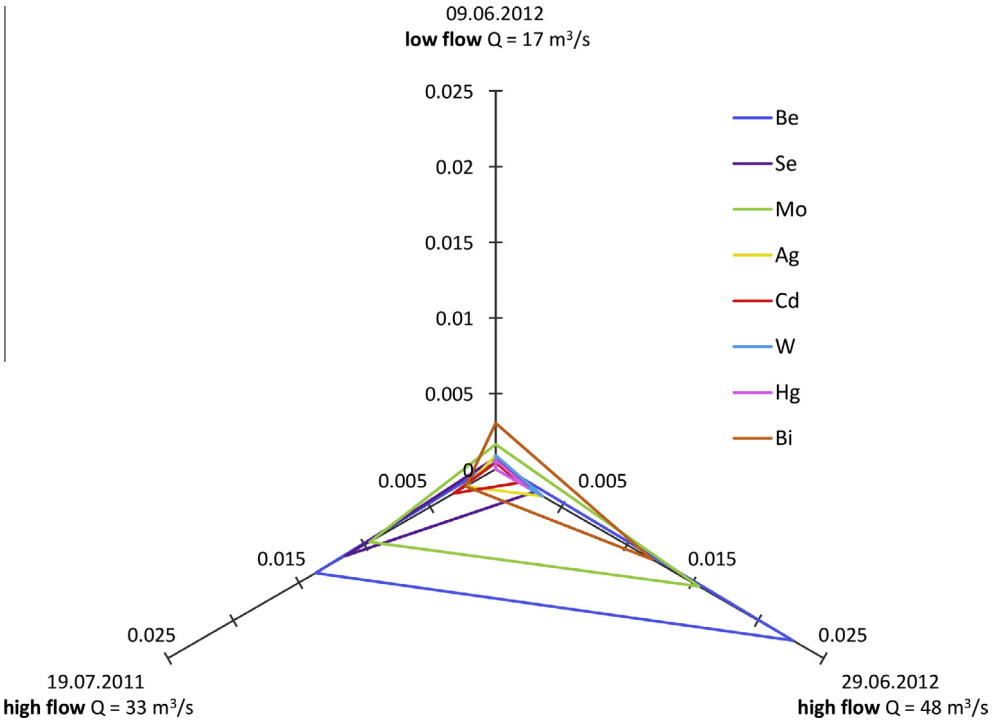

Fig. 9. Observed changes in heavy metal concentrations (mg/l) during high flow events in 2011 and 2012 in the Tuul River at the Ulan Bator gauging station; source of the data: personal field measurements related to the Zaamar filed campaigns in 2011 and 2012.

base scenario (−1.0 kt/year/km). Overall, the base scenario and its observation-based assumption regarding the bed composition results in net storage changes that are much more similar to independent observations in similar rivers (Walling et al., 1998; López-Tarazón et al., 2012) than the changes from the scenarios. A possible explanation is that the base scenario conditions might be more common than the alternative scenario conditions.

Observations of clockwise hysteresis are commonly interpreted as being due to the remobilisation of fresh and readily available in-channel deposits that act as sediment sources (Klein, 1984; Smith and Dragovich, 2009). This process often occurs at the beginning of a hydrological event, when sufficient material has accumulated on the channel bed during the pre-event period (Salant et al., 2008). Hence, due to the extensive erosion of this material, clockwise hysteresis is commonly related to significant increases in sediment loads early in an event (Pentz and Kostaschuk, 1999; Miller and Villarroel, 2011). We here show that such hysteresis behaviour can be reproduced by the present modelling approach, which allows for deposition and erosion along an extensive (127 km) adaptation reach upstream of the (14 km) focus reach.

Observations of anti-clockwise hysteresis loops during flow events, with their characteristic delay in the sediment concentration peak relative to the flow peak, are commonly taken as evidence of delayed input of relatively remote sediments from catchment processes, such as hillslope erosion during rainfall events (Bača, 2008; Oeurng et al., 2010; Megnounif et al., 2013). Such processes can be modelled with soil erosion models (Sander et al., 2011) that use precipitation data as input (e.g., Hughes et al., 2012). Importantly, this study shows that the delay in the sediment concentration peak relative to the flow peak may be equally well explained by delayed input from upstream in-channel processes (in our case, from the modelled adaptation reach). This result emphasises that observations of anti-clockwise hysteresis alone cannot provide conclusive evidence of on-going catchment processes such as hillslope erosion. Furthermore, the present results show that the model can reproduce anti-clockwise hysteresis loops that occur both under conditions of limited bed sediment availability resulting in net deposition, as independently observed by Lefrançois et al. (2007), and under conditions of more abundant sediment availability resulting in net erosion (López-Tarazón et al., 2009).

Empirical relations between historically observed sediment concentrations and discharges (sediment rating curves) are often used in sediment transport quantifications as an alternative to more complex numerical modelling of events when relevant direct concentration measurement results are lacking (e.g., Benjankar and Yager, 2012). However, hysteresis effects can be considerable in some natural steams, implying weak statistical relations between sediment concentration and water discharge due to data scatter (López-Tarazón et al., 2009). The resulting sediment rating curves in such cases may be too uncertain to be used in sediment load predications (Wulf et al., 2012). Because there may be many different causes of such hysteresis and data scatter, such as variation in sediment supplies and seasonal effects (Asselman, 2000), a key challenge is to identify and increase the understanding of dominant hysteresis mechanisms. The present modelling approach enabled the evaluation of the specific contribution of in-channel processes to hysteresis, showing the relatively large influence of these processes in causing data scatter in sediment rating curves, decreasing R^2 from the hypothetical value of unity that would occur in the absence of hysteresis down to values of approximately 0.5 to 0.6. Hence, although there are many different factors that cause hysteresis, the present results indicate that understanding and accounting for in-channel processes alone may considerably improve sediment load predications.

A large fraction of metal contaminants in rivers are commonly transported in a particulate-associated form (Martin and Meybeck, 1979) and follow the same transport pathways as the natural sediments of a river. In the Tuul River, the mostly alkaline water conditions (pH 8.5–9.6) act to further enhance such metal transport with sediment load (Thorslund et al., 2012; Chalov

et al., 2015). Furthermore, the observed absolute metal concentrations in the suspended sediments of the Tuul River at the Ulan Bator gauging station increased significantly during high flow events in 2011 and 2012 (Fig. 9). A possible explanation for this is that the prevalence of certain, more contaminated particle size fractions can increase during event flows (Kurtenbach and Krein, 2007). Specifically, the results of the present model of the Tuul River indicated that relatively fine particles (0.062–0.25 mm; particle size 1) eroded preferentially over coarser particles during the events (e.g., Fig. 4), implying that their prevalence in suspension increased; the pattern in Fig. 9 hence suggests that this fine fraction may be relatively contaminated. Fig. 9 also shows that the overall trends are consistent among the different heavy metals, although the magnitude of change differs. While some heavy metals (Be, Ag and Mo) clearly increased in the high flows, the remainder (Se, Cd, W, Hg and Bi) demonstrated greater variability between the different flow conditions.

This study shows that deposition can occur continuously during relatively long low-flow periods, which means that the deposited material will be stored for a relatively long time. However, the majority of sediment deposition occurs during relatively short high-flow events. Because both deposition and erosion can occur during the same (short) event, sediment deposition can be short term (inter-event). In some cases, huge amounts of material can therefore be stored for short periods of time (up to a few days). Because such short-term deposits of (contaminated) sediments can act as pollution sources when eroded, understanding such dynamics is important for water quality protection planning (Haag et al., 2001; Marttila and Kløve, 2010). For instance, if climate change (Chalov et al., 2015) or other anthropogenic pressures (Bobrovitskaya et al., 2003; Walling 2006) cause increases in the magnitude and number of flow events, as observed in two recent hydrological years (2012 and 2013; Centre of Register of Hydrotechnical Constructions, 2014), the inter-event character of sediment storage may become more pronounced due to enhanced erosional processes (Turowski et al., 2009).

5. Conclusions

- The present modelling approach can reproduce both anti-clockwise and clockwise hysteresis effects through the consideration of in-channel depositional and erosional dynamics along an extensive (127 km) adaptation reach upstream of the (14 km) focus reach from which the results are extracted.
- Overall, the modelling results show that considerable anti-clockwise hysteresis effects can be caused by in-channel processes alone without being reinforced by catchment processes such as hillslope erosion.
- The specific contribution of in-channel processes to hysteresis was found to be relatively large, introducing data scatter into the sediment rating curves and decreasing R^2 from unity to approximately 0.5 to 0.6.
- According to the present modelling approach, the observations of increased riverine concentrations of heavy metals during high flow events in the Tuul River near Ulan Bator could be caused by an increased prevalence of contaminated fine particles during such events.
- The majority of the total sediment deposition occurs during relatively short high-flow events. Because such short-term deposits of (contaminated) sediments were prone to erosion during the same (short) event, they could act as local pollution sources. More generally, possible changes in the number or magnitude of high-flow events, caused by climatic or other anthropogenic factors, could therefore directly influence the spread of pollution.

Acknowledgments

This study was funded through the EU 7th framework programme Marie Curie Action – International Research Staff Exchange Scheme "FLUMEN" (Grant Agreement Number: PIRSES-GA-2012-318969) and the Swedish Research Council Formas (project 2012-790). This study is also part of the project "Hydroclimatic and ecohydrological changes of the Lake Baikal drainage basin", financially supported by a travel grant from the Faculty of Science, Stockholm University. The study has been supported by the Russian Foundation for Basic Research (project number: 12-05-00069-a, 12-05-33090) and the Russian Geographical Society project "Expedition Selenga-Baikal". The field works were additionally implemented under the support of the Russian–Mongolian biological expedition RAS-MAS with a Russian geographical society grant "Expedition Selenga–Baikal", from the Russian Foundation for Basic Research (project number: 15-05-05515, 15-05-03752). Analytical part of the work was supported by Russian Scientific Foundation, project 14-17-00155 "River runoff parameterization for prediction of hydrological hazards and their environmental consequences". In addition, we gratefully acknowledge the support in the form of discharge data provided by Dr G. Davaa, director of the Hydrology Division of the Mongolian Institute of Meteorology and Hydrology.

Appendix A. Supplementary material

Supplementary data associated with this article can be found, in the online version, at http://dx.doi.org/10.1016/j.jhydrol.2015.05.009. These data include Google maps of the most important areas described in this article.

References

Adams, K.D., Chen, L., 2010. Historic erosion and sediment delivery to Walker Lake from Lake-level lowering: implication for the Lower Walker River and Walker Lake under increased flows; project E. In: Collopy, M.W., Thomas, J.M. (Eds.), Restoration of a Desert Lake in an Agriculturally Dominated Watershed: The Walker Lake Basin, Walker Basin Project. University of Nevada, Reno.

Alexeevsky, N.I., 1998. Forming and Transport of River Sediments. MSU Publishing House, Moscow, pp. 1–203 (in Russian).

Alexeevsky, N.I., Chalov, R.S., Berkovich, K.M., Chalov, S.R., 2013. Channel changes in largest Russian rivers: natural and anthropogenic effects. Int. J. River Basin Manage. 11 (2), 175–191. http://dx.doi.org/10.1080/15715124.2013.814660.

Altansukh, O., 2008. Surface quality assessment and modeling. A case study in the Tuul River, Ulaanbaatar city, Mongolia, M.Sc. Thesis. International Institute for Geo-Information Science and Earth Observation, Enschiede.

Arcement, G.J., Jr., Schneider, V.R., 1984. Guide for selecting manning's roughness coefficients for natural channels and flood plains. USGS, Water-Supply Paper 2339, Denver.

Asselman, N.E.M., 2000. Fitting and interpretation of sediment rating curves. J. Hydrol. 234 (3–4), 228–248.

Asselman, N.E.M., van Wijngaarden, M., 2002. Development and application of a 1D floodplain sedimentation model for the River Rhine in The Netherlands. J. Hydrol. 268 (1–4), 127–142. http://dx.doi.org/10.1016/S0022-1694(00)00253-5.

Bača, P., 2008. Hysteresis effect in suspended sediment concentration in the Rybárik basin, Slovakia/Effet d'hystérèse dans la concentration des sédiments en suspension dans le bassin versant de Rybárik (Slovaquie). Hydrol. Sci. J. 53 (1), 224–235. http://dx.doi.org/10.1623/hysj.53.1.224.

Battulga, P., Dae, P.Y., Senjim, B., Tsagaantsooj, N., 2009. The impact of forest degradation in Tuul river basin's surface water resources. In: Tanaka, T., Jayakumar, R., Erdenechimeg, G. (Eds.), Proceedings of UNESCO Chair Workshop on Sustainable Groundwater Management in Arid and Semi-arid Regions, IHP VII Technical Documents in Hydrology, No. 1. UNESCO, Beijing, pp. 57–64.

Benjankar, R., Yager, E.M., 2012. The impact of different sediment concentrations and sediment transport formulas on the simulated floodplain processes. J. Hydrol. 450–451, 230–243. http://dx.doi.org/10.1016/j.jhydrol.2012.05.009.

Berezhnykh, T.V., Marchenko, O.Y., Abasov, N.V., Mordvinov, V.I., 2012. Changes in the summertime atmospheric circulation over East Asia and formation of long-lasting low-water periods within the Selenga river basin. Geogr. Nat. Resour. 33 (3), 223–229. http://dx.doi.org/10.1134/S1875372812030079.

Bobrovitskaya, N.N., Kokorev, A.V., Lemeshko, N.A., 2003. Regional patterns in recent trends in sediment yields of Eurasian and Siberian rivers. Global Planet Change 39 (1–2), 127–146. http://dx.doi.org/10.1016/S0921-8181(03)00021-3.

Byambaa, B., Todo, Y., 2011. Technological impact of placer gold mine on water quality: case of Tuul River Valley in Zaamar Goldfield, Mongolia. IJEE 75, 167–175.
Bull, L.J., 1997. Relative velocities of discharge and sediment waves for the River Severn, UK. Hydrol. Sci. J. 42 (5), 649–660. http://dx.doi.org/10.1080/02626669709492064.
Camenen, , Larroudé, P., B.T., 2003. Comparison of sediment transport formulae for the coastal environment. Coast. Eng. 48 (2), 111–132. http://dx.doi.org/10.1016/S0378-3839(03)00002-4.
Centre of Register of Hydrotechnical Constructions, 2014. <http://www.waterinfo.ru/> (accessed 25.03.14).
Chalov, S.R., Jarsjö, J., Kasimov, N.S., Romanchenko, A., Pietroń, J., Thorslund, J., Belozerova, E., 2015. Spatio-temporal variation of sediment transport in the Selenga River Basin, Mongolia and Russia. Environ. Earth Sci. 73 (2), 663–680. http://dx.doi.org/10.1007/s12665-014-3106-z.
Chalov, S.R., 2014. Effects of placer mining on suspended sediment budget: case study of north of Russia's Kamchatka Peninsula. Hydrol. Sci. J. 59 (5), 1081–1094. http://dx.doi.org/10.1080/02626667.2014.903330.
Ciszewski, D., 2001. Flood-related changes in heavy metal concentrations within sediments of the Biała Przemsza River. Geomorphology 40 (3–4), 205–218. http://dx.doi.org/10.1016/S0169-555X(01)00044-7.
Cofalla, C., Hudjetz, S., Roger, S., Brinkmann, M., Frings, R., Wölz, J., Schmidt, B., Schäffer, A., Kammann, U., Hecker, M., Hollert, H., Schüttrumpf, H., 2012. A combined hydraulic and toxicological approach to assess re-suspended sediments during simulated flood events—part II: an interdisciplinary experimental methodology. J. Soils Sediments 12 (3), 429–442. http://dx.doi.org/10.1007/s11368-012-0476-2.
Davaa, G., 2012. Hydrology Division of Mongolia Institute of Meteorology and Hydrology, personal communication.
Davaa, G., Odgarav, J., 2012. Tuul River. In: Chikamori, H., Liu, H., Daniell, T. (Eds.), Catalogue of Rivers for Southeast Asia and the Pacific –, vol. VI. UNESCO-IHP Regional Steering Southeast Asia and the Pacific Committee for Southeast Asia and the Pacific.
Destouni, G., Hannerz, F., Prieto, C., Jarsjö, J., Shibuo, Y., 2008. Small unmonitored near-coastal catchment areas yielding large mass loading to the sea. Global Biogeochem. Cycles 22 (4), 1–10. http://dx.doi.org/10.1029/2008GB003287.
Destouni, G., Jaramillo, F., Prieto, C., 2013. Hydroclimatic shifts driven by human water use for food and energy production. Nat. Clim. Change 3, 213–217. http://dx.doi.org/10.1038/nclimate1719.
El kadi Abderrezzak, K., Paquier, A., 2009. One-dimensional numerical modeling of sediment transport and bed deformation in open channels. Water Resour. Res. 45 (5), 1–20. http://dx.doi.org/10.1029/2008WR007134.
Fan, X., Shi, C., Shao, W., Zhou, Y., 2013. The suspended sediment dynamics in the Inner-Mongolia reaches of the upper Yellow River. Catena 109, 72–82. http://dx.doi.org/10.1016/j.catena.2013.05.010.
Ferrington, J., 2000. Environmental problems of placer gold mining in the Zaamar Goldfield, Mongolia. World Placer J. 1, 107–128.
Garmaev, E.J., Khristovorov, A.V., 2010. Water Resources of the Rivers of the Lake Baikal Basin: Basics of Their Use and Protection. Academic Press "Geo", Novosibirsk.
Gibson, S., Brunner, G., Piper, S., Jensen, M., 2006. Sediment Transport Computation with HEC-RAS. In: Proceedings of Eighth Federal Interagency Sedimentation Conference (8thFISC). Reno, pp. 57–64.
Gibson, S., Pak, J., Fleming, M., 2010. Modeling watershed and riverine sediment processes with HEC-HMS and HEC-RAS, Watershed Management 2010. American Society of Civil Engineers, pp. 1340–1349. http://dx.doi.org/10.1061/41143(394)120.
Graf, W.L., 1996. Transport and deposition of plutonium-contaminated sediments by fluvial processes, Los Alamos Canyon, New Mexico. Geol. Soc. Am. Bull. 108 (10), 1342–1355. http://dx.doi.org/10.1130/0016-7606(1996)108<1342:TADOPC>2.3.CO;2.
Haag, I., Kern, U., Westrich, B., 2001. Erosion investigation and sediment quality measurements for a comprehensive risk assessment of contaminated aquatic sediments. Sci. Total Environ. 266 (1–3), 249–257. http://dx.doi.org/10.1016/S0048-9697(00)00753-1.
Herman, W.A., Roessler, C., Robinson, J., 2007. Sediment transport in sand bed streams – Cape Fear 04 River Basin. North Carolina Department of Environment and Natural Recourses Ecosystem Enhancement Program, Ecosystem Enhancement Program. Baker Engineering, Cary.
Hudson, P.F., 2003. Event sequence and sediment exhaustion in the lower Panuco Basin, Mexico. Catena 52 (1), 57–76. http://dx.doi.org/10.1016/S0341-8162(02)00145-5.
Hughes, A.O., Quinn, J.M., McKergow, L.A., 2012. Land use influences on suspended sediment yields and event sediment dynamics within two headwater catchments, Waikato, New Zealand. New Zeal. J. Mar. Fresh. 46 (3), 315–333. http://dx.doi.org/10.1080/00288330.2012.661745.
Hummel, R., Duan, J.G., Zhang, S., 2012. Comparison of unsteady and quasi-unsteady flow models in simulating sediment transport in an ephemeral Arizona Streams. J. Am. Water Resour. As. 48 (5), 987–998. http://dx.doi.org/10.1111/j.1752-1688.2012.00663.x.
Jarsjö, J., Asokan, S.M., Prieto, C., Bring, A., Destouni, G., 2012. Hydrological responses to climate change conditioned by historic alterations of land-use and water-use. Hydrol. Earth Syst. Sci. 16, 1335–1347. http://dx.doi.org/10.5194/hessd-8-7595-2011.
Jarsjö, J., Shibuo, Y., Destouni, G., 2008. Spatial distribution of unmonitored inland water discharges to the sea. J. Hydrol. 348 (1–2), 59–72. http://dx.doi.org/10.1016/j.jhydrol.2007.09.052.
Klein, M., 1984. Anti clockwise hysteresis in suspended sediment concentration during individual storms: Holbeck catchment; Yorkshire, England. Catena 11 (2–3), 251–257. http://dx.doi.org/10.1016/S0341-8162(84)80024-7.
Kleinhans, M.G., Wilbers, A.W.E., Ten-Brinke, W.B.M., 2007. Opposite hysteresis of sand and gravel transport upstream and downstream of a bifurcation during a flood in the River Rhine, the Netherlands. Geol. Mijnbouw 86, 273–285.
Kurtenbach, A., Krein, A., 2007. Pre-event hydrological condition as determinants for suspended sediment and pollutant transport during artificial and natural floods. In: Westrich, B., Förstner, U. (Eds.), Sediment Dynamics and Pollutant Mobility in Rivers – An Interdisciplinary Approach. Springer, Berlin, pp. 279–287.
Lawler, D.M., Petts, G.E., Foster, I.D., Harper, S., 2006. Turbidity dynamics during spring storm events in an urban headwater river system: the Upper Tame, West Midlands, UK. Sci Total Environ. 360 (1–3), 109–126. http://dx.doi.org/10.1016/j.scitotenv.2005.08.032.
Lefrançois, J., Grimaldi, C., Gascuel-Odoux, C., Gilliet, N., 2007. Suspended sediment and discharge relationships to identify bank degradation as a main sediment source on small agricultural catchments. Hydrol. Process. 21 (21), 2923–2933. http://dx.doi.org/10.1002/hyp.6509.
Lisle, T.E., 1989. Sediment transport and resulting deposition in spawning gravels, north coastal California. Water Resour. Res. 25 (6), 1303–1319. http://dx.doi.org/10.1029/WR025i006p01303.
López-Tarazón, J.A., Batalla, R.J., Vericat, D., Francke, T., 2009. Suspended sediment transport in a highly erodible catchment: the River Isábena (Southern Pyrenees). Geomorphology 109 (3–4), 210–221. http://dx.doi.org/10.1016/j.geomorph.2009.03.003.
López-Tarazón, J.A., Batalla, R.J., Vericat, D., Francke, T., 2012. The sediment budget of a highly dynamic mesoscale catchment: the River Isábena. Geomorphology 138 (1), 15–28. http://dx.doi.org/10.1016/j.geomorph.2011.08.020.
Martin, J.-M., Meybeck, M., 1979. Elemental mass-balance of material carried by major world rivers. Mar. Chem. 7 (3), 173–206. http://dx.doi.org/10.1016/0304-4203(79)90039-2.
Marttila, H., Kløve, B., 2010. Dynamics of erosion and suspended sediment transport from drained peatland forestry. J. Hydrol. 388 (3–4), 414–425. http://dx.doi.org/10.1016/j.jhydrol.2010.05.026.
Megnounif, A., Terfous, A., Ouillon, S., 2013. A graphical method to study suspended sediment dynamics during flood events in the Wadi Sebdou, NW Algeria (1973–2004). J. Hydrol. 497, 24–36.
Miller, J.R., Villarroel, L.F., 2011. Bolivia: mining, river contamination and human health. In: Nriagu, J.O. (Eds.), Encyclopedia of Environmental Health. Elsevier, pp. 421–441.
Młynarczyk, Z., 1996. Acta Quaternaria 1: Transport materiału piaszczystego w korycie rzeki meandrującej i krętej (na przykładzie środkowej Prosny). Wyd, Naukowe UAM, Poznań (in Polish).
Nadal-Romero, E., Regüés, D., Latron, J., 2008. Relationships among rainfall, runoff, and suspended sediment in a small catchment with badlands. Cetena 74 (2), 127–136. http://dx.doi.org/10.1016/j.catena.2008.03.014.
Oeurng, C., Sauvage, S., Sánchez-Pérez, J.-M., 2010. Dynamics of suspended sediment transport and yield in a large agricultural catchment, southwest France. Earth Surf. Proc. Land. 35 (11), 1289–1301. http://dx.doi.org/10.1002/esp.1971.
Ollivier, P., Hamelin, B., Radakovitch, O., 2010. Seasonal variations of physical and chemical erosion: a three-year survey of the Rhone River (France). Geochim. Cosmochim. 74 (3), 907–927. http://dx.doi.org/10.1016/j.gca.2009.10.037.
Owens, P.N., Walling, D.E., Leeks, G.J.L., 1999. Deposition and storage of fine-grained sediment within the main channel system of the River Tweed, Scotland. Earth Surf. Proc. Land. 24 (12), 1061–1076. http://dx.doi.org/10.1002/(SICI)1096-9837(199911)24:12<1061::AID-ESP35>3.0.CO;2-Y.
Pentz, S.B., Kostaschuk, R.A., 1999. Effect of placer mining on suspended sediment in reaches of sensitive fish habitat. Environ. Geol. 37 (1–2), 78–89. http://dx.doi.org/10.1007/s002540050363.
Pereira, J.F., McCorquodale, J.A., Meselhe, E.A., Georgiou, I.Y., Allison, M.A., 2009. Numerical simulation of bed material transport in the lower Mississippi River. J. Coast. Res. 56, 1449–1453.
Punsalmaa, B., Nyamsuren, B., Buyndalai, B., 2004. Trends in River and Lake Ice in Monoglia. AIACC Working Paper 4. <http://arigsormn.blogspot.se/2012/06/trends-in-river-and-lake-ice-in.html>.
Runkui, L., A-Xing, Z., Sianfeng, S., Ming, C., 2010. Seasonal dynamics of runoff-sediment relationship and its controlling factors in black soil region of Northeast China. J. Resour. Ecol. 1 (4), 345–352. http://dx.doi.org/10.3969/j.issn.1674-764x.2010.04.007.
Salant, N.L., Hassan, M.A., Alonso, C.V., 2008. Suspended sediment dynamics at high and low storm flows in two small watersheds. Hydrol. Process. 22, 1573–1587. http://dx.doi.org/10.1002/hyp.6743.
Sander, G.C., Zheng, T., Heng, P., Zhong, Y., Barry, D.A., 2011. Sustainable soil and water resources: modelling soil erosion and its impact on the environment. In: 19th International Congress on Modelling and Simulation (Modsim2011), pp. 45–56.
Shimarayev, M.N., Starygina, L.N., 2010. Lake Baikal: zonal atmospheric circulation, climate and hydrological processes (1968–2007). Geogr. Nat. Resour. 31 (3), 245–250.

Sloto, R.A., Couse, M.Y., 1996. HYSEP: a Computer Program for Stream Flow Hydrograph Separation and Analysis, Water Resources Investigation Report 96–4040. USGS, Lemoyne.

Smith, B.P.G., Naden, P.S., Leeks, G.J.L., Wass, P.D., 2003. The influence of storm events on fine sediment transport, erosion and deposition within a reach of the River Swale, Yorkshire, UK. Land Ocean interaction: processes, functioning and environmental management: a UK perspective. Sci. Total Environ. 314–316, 451–474. http://dx.doi.org/10.1016/S0048-9697(03)00068-8.

Smith, H.G., Dragovich, D., 2008. Sediment budget analysis of slope–channel coupling and in-channel sediment storage in an upland catchment, southeastern Australia. Geomorphology 101 (4), 643–654. http://dx.doi.org/10.1016/j.geomorph.2008.03.004.

Smith, H.G., Dragovich, D., 2009. Interpreting sediment delivery processes using suspended sediment-discharge hysteresis patterns from nested upland catchments, south–eastern Australia. Hydrol. Process. 23 (17), 2415–2426. http://dx.doi.org/10.1002/hyp.7357.

Stubblefield, A., Chandra, S., Eagan, S., Tuvshinjargal, D., Davaadorzh, G., Gilroy, D., Sampson, J., Thorne, J., Allen, B., Hogan, Z., 2005. Impacts of gold mining and land use alterations on the water quality of central Mongolian rivers. Integr. Environ. Assess. Manage. 1 (4), 365–373.

Thorslund, J., Jarsjö, J., Chalov, S.R., Belozerova, E.V., 2012. Gold mining impact on riverine heavy metal transport in a sparsely monitored region: the upper Lake Baikal Basin case. J. Environ. Monit. 14 (10), 2780–2792. http://dx.doi.org/10.1039/c2em30643c.

Törnqvist, R., Jarsjö, J., Karimov, B., 2011. Health risks from large-scale water pollution: trends in Central Asia. Environ. Int. 37, 435–442. http://dx.doi.org/10.1016/j.envint.2010.11.006.

Törnqvist, R., Jarsjö, J., Pietroń, J., Bring, A., Rogberg, P., Asokan, S.M., Destouni, G., 2014. Evolution of hydro-climate system in the Lake Baikal basin. J. Hydrol. 519, 1953–1962. http://dx.doi.org/10.1016/j.jhydrol.2014.09.074.

Törnqvist, R., Jarsjö, J., Thorslund, J., Rao, P.S.C., Basu, N.B., Destouni, G., 2015. Mechanisms of basin-scale nitrogen load reductions under intensified irrigated agriculture. PLoS One 10 (3), e0120015. http://dx.doi.org/10.1371/journal.pone.0120015.

Turowski, J.M., Yager, E.M., Badoux, A., Rickenmann, D., Molnar, P., 2009. The impact of exceptional events on erosion, bedload transport and channel stability in a step-pool channel. Earth Surf. Process. Land. 34 (12), 1661–1673. http://dx.doi.org/10.1002/esp.1855.

USACE, 1993. HEC-6 User's Manual. U.S. Army Corps of Engineers Centre, Davis, pp. 7–33.

USACE, 2010a. HEC-RAS river analysis system. User's Manual Ver. 4.1. U.S. Army Corps of Engineers Centre, Davis.

USACE, 2010b. HEC-RAS river analysis system, hydraulic reference manual Ver. 4.1. U.S. Army Corps of Engineers Centre, Davis.

USGS, 2012a. Earth Explorer. <http://earthexplorer.usgs.gov/> (accessed 20.01.12).

USGS, 2012b. Global Visualization Viewer. <http://glovis.usgs.gov/>. (accessed 22.02.12).

Walling, D.E., 2006. Human impact on land–ocean sediment transfer by the world's rivers. Geomorphology 79 (3–4), 192–216. http://dx.doi.org/10.1016/j.geomorph.2006.06.019.

Walling, D.E., Owens, P.N., Leeks, G.J.L., 1998. The role of channel and floodplain storage in the suspended sediment budget of the River Ouse, Yorkshire, UK. Geomorphology 22 (3–4), 225–242. http://dx.doi.org/10.1016/S0169-555X(97)00086-X.

Williams, G.P., 1989. Sediment concentration versus water discharge during single hydrologic events in rivers. J. Hydrol. 111 (1–4), 89–106. http://dx.doi.org/10.1016/0022-1694(89)90254-0.

Wulf, H., Bookhagen, B., Scherler, D., 2012. Climatic and geologic controls on suspended sediment flux in the Sutlej River Valley, western Himalaya. Hydrol. Earth Syst. Sci. 16 (7), 2193–2217. http://dx.doi.org/10.5194/hess-16-2193-2012.

Yang, C.T., 2002. Sediment transport modelling – combination of theoretical concepts and practical approach. In: Summer, W., Walling, D.E. (Eds.), International Hydrological Program, Modeling Erosion, Sediment Transport and Sediment Yield, IHP-VI Technical Documents in Hydrology. UNESCO, Paris, pp. 101–136.

Zhang, S., Duan, J.G., 2011. 1D finite volume model of unsteady flow over mobile bed. J. Hydrol. 405 (1–2), 57–68. http://dx.doi.org/10.1016/j.jhydrol.2011.05.010.